Embedding molecular dynamics within fluctuating hydrodynamics in multiscale simulations of liquids

R. Delgado-Buscalioni[1,*] and G. De Fabritiis[2,†]

[1] *Depto. Física Teorica de la Materia Condensada, Universidad Autónoma de Madrid, Campus de Cantoblanco, Madrid, E-28049, Spain.*

[2] *Computational Biochemistry and Biophysics Laboratory (GRIB-IMIM), Universitat Pompeu Fabra, Barcelona Biomedical Research Park (PRBB), C/ Dr. Aiguader 88, 08003, Barcelona, Spain*

(Dated: July 4, 2007)

We present a hybrid protocol designed to couple the dynamics of a nanoscopic region of liquid described at atomistic level with a fluctuating hydrodynamics description of the surrounding liquid. The hybrid technique is based on the exchange of fluxes and it is shown to respect the conservation laws of fluid mechanics. This fact allows to solve unsteady flows involving shear and sound waves crossing the interface of both domains. In equilibrium we find perfect agreement with the Grand-Canonical ensemble at low and moderate densities, while within the nanoscopic volumes considered, mass fluctuation (both in hybrid and full MD simulations) becomes slightly larger than predicted by the thermodynamic limit. Stress fluctuations across the hybrid interface are shown to have a seamless profile. Non-equilibrium scenarios involving shear (start-up of Couette flow) and longitudinal flow (sound waves) are also illustrated.

I. INTRODUCTION

Multiscale modeling has been rapidly evolving during the last decade, and it now constitutes a new paradigm in computer simulation to resolve systems and processes comprising different length scales. The essence of a multiscale, multi-physics approach consists in using different model descriptions for each relevant scale. Importantly, information has to be able to feed-back and forward between different scales and models. In many instances, multiscale simulations can be performed in a hierarchical way, i.e. by extracting information from one scale as input parameters for the higher level model. Relevant examples of this procedure are the coarse-graining techniques which start from atomistic simulations to produce simplified coarse-grained representations of complex molecules used for the study of equilibrium properties of complex fluids [1]. However, many processes take place as a consequence of the continuous interaction between elements pertaining to different spatio-temporal scales. These sort of processes require another kind of multiscale approach in which the information required for each model needs to be exchanged *on-the-fly*. In this case one can talk about concurrent coupling [2, 3] and hybrid models. Hybrid models are now deployed in many different disciplines, such as quantum-classical treatment of solid fractures [4], plasma physics [5], rarefied gases [6], complex liquids [7–9], turbulence, and more. A list which cannot be exhaustive.

In this work, we focus on hybrid models for the liquid phase coupling two domains described respectively by atomistic and continuum descriptions (domain decomposition). In general, hybrid models in the liquid phase can be divided in two groups: either based on an Eulerian-Lagrangian decomposition [8, 9] or on domain decomposition [7, 10]. The Eulerian-Lagrangian approach consists in modelling solute particles as Lagrangian objects moving in a Eulerian fluid description and is useful for phenomena involving the bulk flow of complex fluids. Domain decomposition is meant to provide an accurate atomistic representation of a small relevant region of the system, for instance at a molecular interface or around a macromolecule, embedded into a coarser mesoscopic description of matter [10]. This area has received multiple contributions during the last decade or so (for a recent review we refer to Ref. [7]). In general terms, previous works on this subject have focused on how the mean flow profiles at the bulk are affected by the discrete nature of matter near boundary regions (e.g., near walls [11] or contact lines [12]). Consequently, in these works accurate atomistic representation of the particle system was not considered, and particles were usually described using the standard coarse-grained Lennard-Jones model. In these scenarios, flow are driven by shear stress and the large time separation between the molecular domain and the fluid bulk enables the assumption of stationary process. In this sense, some groups have used the Schwartz method (variable coupling) [7] as a fast way to reach the stationary state, by consecutively imposing the mean velocity field at the hybrid border (overlapping region) towards and from the particle and continuum domains. Being interested in mean flow features, fluctuations, naturally arising from the particle system, have been usually considered as a nuisance (with the exception, in gases, of the works by Garcia's group [13]). Methods to control the noise-to-signal ratio have been consequently proposed in the literature [14, 15].

In Ref. [10] the coupled protocol used for hybrid molecular dynamics simulations has been sketched to study the reflection of sound waves of water against a lipid monolayer (dimyristoylphosphatidylcholine, DMPC) by

*rafael.delgado@uam.es

†gianni.defabritiis@upf.edu

the introduction of a hybrid method designed to bridge nanoscopic and microscopic molecular scales (hybrid MD). One important objective of the present hybrid model is to enable the study of the effects of external flow in a nanoscopic region and in its molecular structure which required the inclusion of important features not readily available in the literature. We also showed that the hybrid code is able to capture small differences in the bulk arising from a particular molecular structure far away, at the lipid interface. In this work we finally present the detailed explanation of the coupled protocol and focus in the treatment of fluctuations of mass, momentum and pressure tensor. Instead of working with TIP3P water as in [10] which is restricted to ambient conditions (T=300K and 1 atm), we work here with argon enabling us to study the effect of the hybrid protocol on the density, as it changes from gas to dense liquid phase, ρ =0.1 to 0.8 gr/(mol$\mathring{A}^3$). We also provide some extra tools, quite useful for calibration purposes in the appendices. At these small scales, time separation can not be taken per granted and thus the hybrid model needs to be able to solve non-stationary flows, including transport of shear stress and sound waves. To that end, we use a scheme based on the exchange of fluxes, which correctly deals with non-stationary flows by respecting the conservation laws of fluid mechanics. Fluctuations are relevant at these scales, being moreover responsible of many different kind of processes. In order to include fluctuations into the coupled model, the continuum domain has to be described, at least, by fluctuating hydrodynamics (FH) [16]. A detail account of the FH model used in this work was recently presented [17]. An important point here is that the inclusion of fluctuations in the hybrid description requires thermodynamic consistency between both MD and FH models. In this sense, the MD system is viewed here as an open system which exchange mass, energy and momentum with the exterior world [18].

In what follows we briefly present, in Sec. II, the fluctuating hydrodynamics and the molecular dynamics models . The core of the coupling method, both in space and in time are presented next in Secs. III and IV. The behaviour of the model at equilibrium is shown in Sec. V and non-equilibrium flows are illustrated in Sec. VI. Finally, some conclusions are given in Sec. VII.

II. MESOSCOPIC AND MOLECULAR DESCRIPTIONS

A. Fluctuating hydrodynamics level

The hydrodynamic behaviour of the mesoscale is described by the fluctuating hydrodynamic (FH) equations [16, 19]. These are stochastic partial differential equations which reduce to the Navier-Stokes equations in the limit of large volumes. Fluctuating hydrodynamics are based on conservation equations of the form $\partial_t \phi(\mathbf{r},t) = -\boldsymbol{\nabla}\cdot\mathbf{J}^{\phi}$, where ϕ is the density of any conserved quantity (mass, momentum, energy) and $\boldsymbol{J}^{\phi}$ is the flux of the conserved quantity. In [17], we considered an isothermal fluid, so that the conserved quantities are reduced to mass and momentum, whose densities are $\rho(\mathbf{r},t)$ and $\boldsymbol{g}(\mathbf{r},t)$ respectively. The corresponding fluxes are,

$$\boldsymbol{J}^{\rho} = \boldsymbol{g}\boldsymbol{v}, \tag{1}$$

$$\boldsymbol{J}^{\boldsymbol{g}} = \left(\boldsymbol{g}\boldsymbol{v} + \boldsymbol{\Pi} + \widetilde{\boldsymbol{\Pi}}\right), \tag{2}$$

where the velocity $\boldsymbol{v}$ field satisfies $\boldsymbol{g} = \rho\boldsymbol{v}$ and $\boldsymbol{J}^{\rho}$, $\boldsymbol{J}^{\boldsymbol{g}}$ are the mass flux vector and the pressure tensor respectively. The pressure tensor in Eq. (2) contains the convection term $\boldsymbol{g}\boldsymbol{v}$ and the stress tensor, divided in a deterministic (mean) and a fluctuating part: $\boldsymbol{\Pi}(\mathbf{r},t)$ and $\widetilde{\boldsymbol{\Pi}}(\mathbf{r},t)$, respectively The deterministic part of the stress tensor corresponds to that of a Newtonian fluid,

$$\boldsymbol{\Pi} = (p+\pi)\mathbf{1} + \overline{\boldsymbol{\Pi}}^{S} \tag{3}$$

where p is the equilibrium thermodynamic pressure given by the equation of state while the trace and traceless symmetric part of the stress tensor are, respectively,

$$\pi = -\zeta\partial_\gamma v_\gamma \tag{4}$$

$$\overline{\Pi}^{S}_{\alpha\beta} = -\eta\left(\partial_\alpha v_\beta + \partial_\beta v_\alpha - 2D^{-1}\partial_\gamma v_\gamma \delta_{\alpha\beta}\right) \tag{5}$$

where the convenion of summation on repeated indexes is used. The shear and bulk viscosities are η and ζ respectively and D is the spatial dimensionality (in our case $D=3$). The fluctuating stress tensor $\widetilde{\Pi}_{\alpha\beta}$ appearing in Eq. (2) is a random Gaussian matrix with zero mean and correlations (see Ref.[16])

$$\langle\widetilde{\Pi}_{\alpha\beta}(\mathbf{r}_1,t_1)\widetilde{\Pi}_{\delta\gamma}(\mathbf{r}_2,t_2)\rangle = 2k_BTC_{\alpha\beta\gamma\delta}\delta(t_1-t_2)\delta(\mathbf{r}_1-\mathbf{r}_2) \tag{6}$$

where $C_{\alpha\beta\gamma\delta} = \left[\eta(\delta_{\alpha\delta}\delta_{\beta\gamma}+\delta_{\alpha\gamma}\delta_{\beta\delta}+(\zeta-\frac{2}{D}\eta)\delta_{\alpha\beta}\delta_{\delta\gamma}\right]$, k_B is the Boltzmann's constant and T the temperature.

The discrete equations of the finite volume discretization of FH of Ref. [17] are included here below for the sake of completeness. The change of mass dM_k^t and momentum $d\boldsymbol{P}_k^t$ in cell k at time t are given by,

$$dM_k^t = \sum_l \boldsymbol{g}_{kl}\cdot\boldsymbol{e}_{kl}A_{kl}dt, \tag{7}$$

$$d\boldsymbol{P}_k^t = \sum_l \left\{\boldsymbol{v}_{kl}\mathbf{g}_{kl} + \frac{(p_l+\pi_l)+\overline{\boldsymbol{\Pi}}_l^S}{2}\right\}\cdot\mathbf{e}_{kl}A_{kl}dt + d\widetilde{\mathbf{P}}_k^t \tag{8}$$

where V_k is the volume of cell k, $\boldsymbol{e}_{kl}$ is the unit vector perpendicular to the contact surface of area A_{kl} from volume k to volume l (in our regular lattice $A_{kl}=A$ is fixed). Note that summations in Eqs. (7) and (8) are done over all the $\{l\}$ control cells that are in contact with cell k. In eqs. (7) and (8) one needs to use the discrete

version of the pressure tensor components introduced in Eqs. (4) and (5); these are,

$$\pi_k = \frac{\zeta}{V_k}\sum_l \frac{A_{kl}}{2} e_{kl}^{\beta} v_l^{\beta}, \tag{9}$$

$$\left[\overline{\mathbf{\Pi}}_k^S\right]_{\alpha\beta} = \frac{\eta}{V_k}\sum_l \left[\frac{A_{kl}}{2}(e_{kl}^{\alpha} v_l^{\beta} + e_{kl}^{\beta} v_l^{\alpha}) - \frac{\delta^{\alpha\beta}}{D} A_{kl} e_{kl}^{\gamma} v_l^{\gamma}\right]$$

Finally, as shown in Refs. [20, 21] the momentum contribution of the fluctuating stress can be evaluated from,

$$\begin{aligned} d\widetilde{\boldsymbol{P}}_k^t &= \sum_l \frac{A_{kl}}{2}\sqrt{4k_B T\frac{\eta}{V_l}}\, d\overline{\mathbf{W}}_l^S \cdot \mathbf{e}_{kl} \\ &+ \sum_l \frac{A_{kl}}{2}\sqrt{2Dk_B T\frac{\zeta}{V_l}}\,\frac{tr[d\mathbf{W}_l]}{D}\mathbf{e}_{kl}, \end{aligned} \tag{10}$$

where $d\mathbf{W}_l$ is a $D \times D$ matrix ($D = 3$ in three dimensions) of independent Wiener increments satisfying $\langle d\mathbf{W}_k^{\alpha,\beta} d\mathbf{W}_l^{\gamma,\delta}\rangle = \delta_{k,l}\delta_{\alpha,\gamma}\delta_{\beta,\delta}dt$ and $d\overline{\mathbf{W}}_l^S$ is a traceless symmetric random matrix defined as

$$d\overline{\mathbf{W}}_l^S = \frac{(d\mathbf{W}_l + d\mathbf{W}_l^T)}{2} - \frac{tr[d\mathbf{W}_l]}{D}\mathbf{1}. \tag{11}$$

For details on the imposition of boundary conditions for the density and momentum we refer to Refs. [17, 22]. As explained below boundary conditions arising from the hybrid coupling are of von Neuman type (for fluxes). When required, solid walls interfacing the FH domain were modelled assuming no-slip boundary condition.

B. Molecular dynamics level

The molecular description is based on classical molecular dynamics. We use the CHARMM27 [23] forcefield incorporating the TIP3P parametrization, which specifies bond, angle, dihedral and improper bonded interactions and non-bonded Lennard-Jones 6-12 and Coulomb interactions. The code is derived from a stripped down version of the molecular dynamics software NAMD [24]. As long as we are working in an isothermal enviroment, thermostatting is needed in the molecular domain. In order to preserve local momentum conservation and the hydrodynamic modes within the molecular domain molecules are thermostated using a dissipative particle dynamics (DPD) thermostat [25]. The DPD thermostat is the best suited for our purposes because it has a negligible effect on the equation of state and the transport coefficients of the fluid.

III. COUPLING METHOD

From a computational point of view the MD and FH domains are solved by two independent binaries which are coupled via a communication service which redirect messages and data between the two codes [2]. The coupling scheme explained below takes place after a fixed time interval Δt_c. In general, we set $\Delta t_c = n_{MD}\delta t = n_{FH}\Delta t$, where n_{MD} and n_{FH} are integers and δt and Δt are the time step of the molecular and hydrodynamic models, respectively. Details of the time stepping protocol are given in section IV.

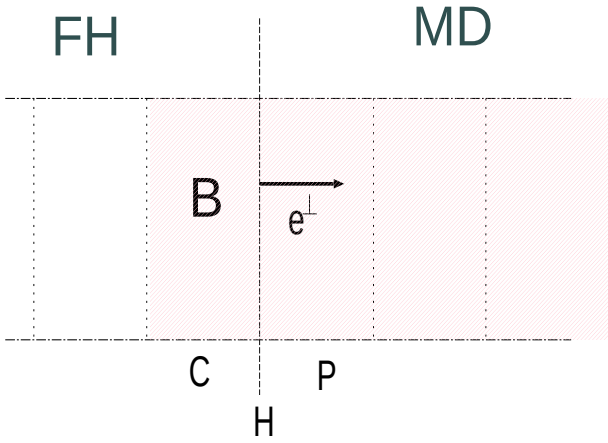

FIG. 1: Geometry of the domain decomposition used in the hybrid scheme. Fluctuating hydrodynamics and molecular dynamics domains, labelled as FH and MD respectively, are separated by the *hybrid* interface H. The shaded area corresponds to the particle region MD+B, where B is the particle buffer. However, the *total* system is uniquely determined by MD+FH.

The MD and FH domains are separated by the *hybrid interface*, which shall be called "H". Figure 1 illustrates a portion of this interface. The whole simulation volume is divided into non-overlapping *control cells* which are used in the finite volume method for fluid dynamics. In Fig. 1 we illustrate the control cells adjacent to the interface H. These cells are called C and P to indicate that they are located at the *continuum* and *particle* side of H, respectively. The region B in Fig. 1 is the particle buffer, which is part of the particle region (in other words, particle region is MD+B). The buffer B is used as a *reservoir* to impose momentum into the MD domain. It is important to note that the *whole system* is the sum of two regions (MD and FH) separated by one single interface H. This provides an unique definition of the global quantities (for instance the overall momentum of the system is $\boldsymbol{P}_{total} = \boldsymbol{P}_{MD} + \boldsymbol{P}_{FH}$). In this way our method provides control of global mass and momentum conservation. By contrasts, the spatial decomposition used in previous hybrid schemes [7] lacks a proper definition of the overall system. This is so because in previous works the particle and continuum domains intertwine within a larger overlapping region, preventing a clear definition of the system (see for instance Refs. [7, 26, 27]).

In order to guarantee mass and momentum conservation, communications are based on flux balance: both domains receive equal (but opposite sign) mass and mo-

mentum currents across the hybrid interface H. As in Ref. [18], in the present scheme mass flux arises naturally from the imposition of the momentum flux (pressure). Thus the flux of momentum across H is the central quantity of the coupling method. We will first explain how this flux is calculated and imposed into the MD system. Then, we comment on how mass conservation and variable continuity are ensured and conclude with the time stepping of the hybrid scheme.

A. Evaluation of the momentum flux across H

Let us now first concentrate on the evaluation of the momentum flux across the hybrid interface, $\boldsymbol{J}_H^{\boldsymbol{g}}$. Using same approximation as in the finite volume scheme momentum flux across H is thus calculated by interpolation from $\boldsymbol{J}_C^{\boldsymbol{g}}$ and $\boldsymbol{J}_P^{\boldsymbol{g}}$, the corresponding values at the adjacent C and P cells, respectively. This gives,

$$\boldsymbol{J}_H^{\boldsymbol{g}} \cdot \boldsymbol{e}_\perp = \frac{\boldsymbol{J}_P^{\boldsymbol{g}} + \boldsymbol{J}_C^{\boldsymbol{g}}}{2} \cdot \boldsymbol{e}_\perp. \tag{12}$$

According to the sense of the vector $\boldsymbol{e}_\perp$ drawn in Fig. 1, Eq.(12) provides the flux of momentum across H towards the P cell. For conservation the flux towards C should be $-\boldsymbol{J}_H^{\boldsymbol{g}}$. In the most general case, $\boldsymbol{J}_P^{\boldsymbol{g}}$ and $\boldsymbol{J}_C^{\boldsymbol{g}}$ are obtained from time averaging over the coupling time Δt_c; details of time average requirements are explained in the Appendix A. We now explain how $\boldsymbol{J}_C^{\boldsymbol{g}}$ and $\boldsymbol{J}_P^{\boldsymbol{g}}$ are evaluated. The C cell belongs to the FH domain so $\boldsymbol{J}_C^{\boldsymbol{g}}$ is directly obtained from Eq. (2). There is, however, a slight difference. The velocity gradient appearing in the local mean stress $\boldsymbol{\Pi}_C$ in Eq. (9) for k =C, requires the local density and velocity of the neighboring l =P cell of the MD domain. These quantities, ρ_P and $\boldsymbol{v}_P$, are obtained from the instantaneous mass and momentum at P,

$$M_P = \sum_{i \in P} m_i \tag{13}$$

$$\boldsymbol{P}_P = \sum_{i \in P} m_i \boldsymbol{v}_i \tag{14}$$

were the summation runs over those molecules at the P cell [46] Dividing by the volume of the P cell V_P one gets the local density $\rho_P = M_P/V_P$; while, as shown in Ref. [28], to recover the correct statistics one needs to evaluate the coarse-grained velocity as $\boldsymbol{v}_P = \mathbf{P}_P/M_P$ instead of from the average of particle velocities.

The momentum flux tensor at P, $\boldsymbol{J}_P^{\boldsymbol{g}}$ can be evaluated by two possible means. First $\boldsymbol{J}_P^{\boldsymbol{g}}$ can be obtained from the "microscopic" state using the Irving-Kirkwood formula,

$$\boldsymbol{J}_P^{\boldsymbol{g}} = \frac{1}{V_P} \langle \sum_{i \in P} m_i \mathbf{v}_i \mathbf{v}_i + \mathbf{W}_i \rangle_{[\delta t_s, \Delta t_c]} \tag{15}$$

where $\mathbf{W}_i = (1/2) \sum_{j \in P} \mathbf{r}_{ij} \cdot \mathbf{f}_{ij}$ being the contribution of atom i to the virial part of the stress tensor [29]. At any time t, the time average in Eq. (15) is defined as follows,

$$\langle \phi \rangle_{[\delta t_s, T]} \equiv \frac{1}{N_s} \sum_{i=1}^{N_s} \phi(t + \delta t_s i) \;\text{ with } T = N_s \delta t_s. \tag{16}$$

As shown in the Appendix A samples of the microscopic stress tensor should be taken each $\delta t_s = 2\tau_c$, where τ_c is the decorrelation time of the stress tensor. This ensures that consecutive samples are uncorrelated and also that the variance of the momentum flux matches at the MD and FH sides.

On the other hand, it is also possible to use a "mesoscopic" route to calculate $\boldsymbol{J}_P^{\boldsymbol{g}}$. In this second approach the momentum flux is evaluated by inserting the local coarse-grained variables at l =P [$\boldsymbol{v}_l = \boldsymbol{P}_P/M_P$ and $\rho_l = M_P/V_P$, where M_P and $\boldsymbol{P}_P$ are given in Eqs. (13) and (14)] and neighboring cells, into Eqs. (2) and (9). The fluctuating part of momentum flux tensor is treated similarly to the other FH cells (Eq. 10). This "mesoscopic" approach is faster because it avoids the costly computation of the virial term. In Sec. V B 4 we show that both ("micro" and "meso") approaches provide similar results in terms of mean and variance of the pressure tensor.

B. Flux boundary conditions

To guarantee momentum conservation after each coupling time Δt_c we need to introduce $\boldsymbol{J}_H^{\boldsymbol{g}} \cdot \boldsymbol{e}_\perp \Delta t_c$ momentum into the MD domain and the opposite of this into the FH domain. This momentum flux can be inserted into the FH domain using standard techniques for the finite volume scheme [17, 22]. In our formulation one only needs the pressure tensor $\boldsymbol{J}^{\boldsymbol{g}}$ at neighboring cells to update the momentum in Eq. (8). In particular for k =C, one just need $\boldsymbol{J}_P^{\boldsymbol{g}}$ from the MD system to close the system of equations for FH cells.

By contrasts, the imposition of the desired momentum flux into the MD system is one of the delicate parts of the coupling scheme. This task is equivalent to impose an external force $\mathbf{F}_H$ introducing the desired input of momentum ($A\boldsymbol{J}_H^{\boldsymbol{g}} \cdot \boldsymbol{e}_\perp \Delta t_c$) into the MD region over the coupling time. To impose this external force we use the particle buffer B (see Fig. 1). Particles are free to enter or leave this buffer across H, but once inside B, each particle $i \in B$ feels an external force $\mathbf{f}_i^{ex}$. The total external force is set to $\sum_{i \in B} \mathbf{f}_i^{ex} = \mathbf{F}_H$, so that the exact amount of pressure and stress is transfered to the *whole* particle system, MD+B. There are several ways to distribute the external force among the (variable) number of particle within the buffer N_B: from the simple equidistribution used in previous works [27] ($\mathbf{f}_i^{ex} = \mathbf{F}_H/N_B$) to much more involved choices considered in Ref.[30]. We discuss this issue in more detail in the Appendix B.

The rôle of the particle buffer is thus to transfer momentum (and more generally energy, see Ref. [18]) into

the MD domain. Each buffer particle acts as a momentum carrier which transfer a part of the force from the outer region. Hence, an important issue is to ensure that there are enough momentum carriers sharing the external force. Otherwise, instabilities could arise due to large particle accelerations at B, arising from large values $\boldsymbol{f}_i^{ex}$. On the other hand, for stability sake and also to reduce the number of particle insertions, it is desirable to control the fluctuations of the number of particles in B, N_B. Both requirements are met by using a simple relaxation algorithm

$$\Delta N_B = (\langle N_B \rangle - N_B)\Delta t/\tau_B, \tag{17}$$

with $\tau_B \simeq 500$ fs. The average number of particles at B, $\langle N_B \rangle$ is set proportional to the mass at the overlapping C cell $M_C = mN_C$: $\langle N_B \rangle = \alpha N_C$. The value of α is not relevant provided that N_B is reasonably large (a good range is $\alpha = [0.5, 0.8]$).

Molecules leaving the buffer cell are simply removed and, if from Eq. (17) $\Delta N_B > 0$ then new molecules are placed in B with a velocity taken from the Maxwellian distribution and $\langle \boldsymbol{v} \rangle = \mathbf{v}_C$, where $\mathbf{v}_C$ is the velocity in the C cell. The insertion location is determined by the USHER algorithm [31, 32], which efficiently finds new molecule configurations releasing an energy equal to the mean energy per molecule. Due to the efficiency of the USHER algorithm, the whole insertion process requires less than few percent of the overall computational time.

In general, momentum exchange due to molecule insertion/removal should be taken into account in the overall momentum balance [18]. The amount of momenta that we want to introduce in the particle system after one MD time step δt is $A\boldsymbol{J}_H^{\boldsymbol{g}} \cdot \boldsymbol{e}_\perp \delta t$. Thus we require that the sum of the contribution of the external force $\boldsymbol{F}_H$ and that of particle insertion/removal satisfy,

$$A\boldsymbol{J}_H^{\boldsymbol{g}} \cdot \boldsymbol{e}_\perp \delta t = \Delta P_{in} - \Delta P_{out} + \boldsymbol{F}_H \delta t. \tag{18}$$

The momentum introduced by incoming particles is $\Delta P_{in} = \sum_i m_i \boldsymbol{v}_i$ (with i being inserted particles during time step δt). In turn ΔP_{out} is the momentum of the particles removed during δt. Equation (18) provides the external force $\boldsymbol{F}_H$ to be imposed over each MD time step δt. Thus, by construction, over each coupling time interval, the exact amount of momentum $A\boldsymbol{J}_H^{\boldsymbol{g}} \cdot \boldsymbol{e}_\perp \Delta t_c$ is transfered to the particle system.

C. Mass transfer and continuity

An important feature of the present scheme is that the mass flux across the hybrid interface H is not imposed, but arises naturally from the pressure gradient and convection across the interface. We note that previous schemes [27, 33] did in fact directly imposed mass injection into the MD system. However, in fluid dynamics, mass flux is not an independent quantity but instead it is controlled by the momentum flux. To be consistent with this fact, we only impose the momentum flux across the hybrid interface and calculate the resulting molecular mass flux across H. Over the coupling time Δt_c, the mass flowing towards C across H is obtained simply by counting the number of molecules crossing the interface. To ensure mass conservation, this amount of mass, ΔM_H^{MD}, is to be injected to the adjacent C cell of the FH model. There is not an unique way to transfer this mass into the C cell; we use the following relaxation equation,

$$\Delta M_C = \Delta M_H^{FH} + \frac{\Delta t_c}{\tau_M}\left(\Delta M_H^{MD} - \Delta M_H^{FH}\right) \tag{19}$$

where τ_M is a relaxation time (we use $\tau_M = 100 n_{FH}$ fs) and $\Delta M_H^{FH} = -A\rho_H \boldsymbol{v}_H \cdot \boldsymbol{e}_\perp \Delta t$ is the mass crossing towards C according to the local hydrodynamic prediction. Thus, in Eq. (19), the mass is relaxed to yield the MD prescription (ΔM_H^{MD}) starting from the hydrodynamic prediction (ΔM_H^{FH}). After releasing the amount of mass ΔM_C in Eq. (19), one needs to update $\Delta M_H^{MD} \to \Delta M_H^{MD} - \Delta M_C$.

Another issue which should be taken into consideration concerns the continuity of velocity across the interface H. Consider a simple Couette flow in a cavity, where the velocity increases linearly with the coordinate normal to the coupling interface. The mean stress tensor is proportional to the velocity gradient which is constant along the cavity. Then it is indeed possible to perfectly match the stress (i.e., the velocity gradient) and still have a discontinuity in the velocity at the H interface. This arises in schemes based on flux-balance and can be solved in two different ways: either adding an extra forcing term in the particle dynamics to ensure that the local mean particle velocity matches the continuum value, or viceversa. The first approach was used in the pioneer work on hybrid coupling by Thomson and O'Connel [34] and it was further modified by some authors [33]. The extra force added to each particle is proportional to the difference between the continuum velocity and the locally averaged particle velocity. We believe that this method is not appropriate because it adds extra *ad hoc* modifications into the molecular dynamics which alter the microscopic dynamic properties.

Instead, as shown in a previous work [15], a better solution is to introduce a relaxation term in the equation for the first continuum cell "C" (see Fig. 1) which ensures that the FH velocity matches the local MD value. We thus add a small relaxation term proportional to $\langle \boldsymbol{v}_H^{MD} \rangle_{[\delta t,\tau]} - \langle \boldsymbol{v}_H^{FH} \rangle_{[\Delta t,\tau]}$ into the momentum equation for the C cell (see Ref. [15]). The values of $\boldsymbol{v}_H^{MD}$ and $\boldsymbol{v}_H^{FH}$ are obtained from the those at the adjacent cells by linear extrapolation. The time averages, defined in Eq. (16), are made over a time τ much smaller than any hydrodynamic time and in these simulations we used $\tau = \Delta t_c$. As demonstrated in Ref. [15], the effect of this relaxing term into the flux balance is negligible.

In summary, in obtaining the mass flux and velocity across the hybrid interface, we assume that the molecular region is the fundamental model from which these

quantities should be evaluated. Mass flux and velocity continuity are thus imposed to the coarse grained fluid model. In this way we avoid the introduction of any extra *ad hoc* artifact into the particle dynamics. In this issue we adhere to the philosophy of Garcia *et al.*, as stated in their elegant hybrid model for gases [6].

IV. THE COUPLING PROTOCOL IN TIME

We now briefly describe the logical flow for the communication process in time used in this implementation of the hybrid model. To start the computational loop one needs the value of the inital momentum flux $\boldsymbol{J}_H^{\boldsymbol{g}}(t_0)$ and the velocity at the interface $\boldsymbol{v}_H$, which are obtained either from the last step of a previous simulation or from the field imposed as initial condition in a new simulation. The time $t_1 = t_0 + \Delta t_c$ is reached upon performing the following steps,

- Step #1. The MD subsystem is moved a number n_{MD} of time steps δt towards $t = t_1$. An external force $\boldsymbol{F}_H$ is imposed at the buffer region B according to what described in Sec.III [see Eq. (18)].

- Step #2. The MD subsystem sends updated information to the FH model. Namely, the momentum flux $\boldsymbol{J}_P^{\boldsymbol{g}}(t_1)$, the total particle mass flowing across H towards C, $\Delta M_H^{MD}(t_1)$ and, the (time averaged) local velocity $\langle \boldsymbol{v}_H(t_1) \rangle_\tau$.

- Step #3. The FH subsystem advances n_{FH} time steps towards $t = t_1$. A momentum flux $-\boldsymbol{J}_H^{\boldsymbol{g}}(t_0) \cdot \boldsymbol{e}_\perp$ is imposed at the boundary H and the mass $\Delta M_H^{MD}(t_1)$ is released into the C cell as according to Eq. (19).

- Step #4. The momentum flux $\boldsymbol{J}_C^{\boldsymbol{g}}(t_1)$ is calculated from the updated FH field. The momentum flux $\boldsymbol{J}_H^{\boldsymbol{g}}(t_1)$ is updated using Eq. (12) and sent to the MD system. The local velocity $\boldsymbol{v}_C$ and mass M_C are also sent towards the MD solver to deal with the buffer dynamics, as explained in Sec. III B. Back to #1 with $t_0 \to t_1$.

The present scheme yields serial coupling and although it is possible to adapt the communications for concurrent coupling (see for instance [3]), we note that for most applications, the hybrid code will not be computationally balanced, as the MD part takes most of the computational time.

The following sections present the results of tests to hybrid model which comprise the study of the equilibrium state and several non-equilibrium unsteady states.

V. RESULTS AT EQUILIBRIUM

A. Mass and momentum conservation.

An important first test to the coupling method is to verify that mass and momentum conservation. To that end we consider an isolated system in equilibrium, with total mass $M = M_{MD} + M_{FH}$ and zero momentum $\boldsymbol{P}_{MD} + \boldsymbol{P}_{FH} = 0$. As stated in Sec. III, the coupling scheme conserves mass by construction. However, as long as the external force is introduced in the buffer B of the particle system, total momentum is exactly conserved in the *extended* system (MD+FD+B). As the buffer volume is small the momentum unbalance is a small bounded quantity of size $|P_B|$. For instance in an isolated system one shall get $\boldsymbol{P}_{MD} + \boldsymbol{P}_{FH} = -\boldsymbol{P}_B$. We checked that after about 1ps, the time average of the overall momentum unbalance per unit mass becomes smaller than the corresponding momentum arising from the thermal noise (see Ref. [10]). Such times are faster than any relevant hydrodynamic time scale and thus momentum unbalance has little effect on the mean and variance of hydrodynamic fields considered. In any case, if required, it is possible to add a slight modification in the coupling scheme which enables *exact* momentum conservation. This is explained in the Appendix C.

B. Equilibrium state

1. Temperature.

By analyzing the behaviour of the hybrid set-up in equilibrium state one can validate the thermodynamic consistency of the coupling method. One first requires a correct temperature imposition because temperature determines momentum fluctuations. The usual way to check the correct thermal behaviour of the model is to evaluate the "numerical" temperature via the equipartition theorem, which relates T to the momentum variance $\langle |\mathbf{P}|^2/M_c \rangle = 3k_BT$ and compare it with the imposed temperature. Here the cell's mass is given by $M_c = \rho V_c$ and $|\mathbf{P}|^2$ is the squared momentum within one cell. As shown in Fig. 2 momentum fluctuations at both FH and MD and cells are in good agreement with the equipartition theorem at the imposed temperature. Momentum fluctuations at the MD cells are consistently controlled by the DPD thermostat, while in the FH domain these are controlled via the fluctuation-dissipation balance [47]. As stated above, in the MD region we used a DPD thermostat [25] to ensure local momentum conservation and maintain the hydrodynamic modes within the molecular region. As an aside Lowe's thermostat [35] was also tested as it also conserves local momentum. However, we observed that for a fixed pressure at the reservoir Lowe's thermostat induces a significant increase in density of the MD domain (about 20%) with respect to the MD

value (obtained in equilibrium simulations within periodic boundaries). By contrast the DPD thermostat is more robust in the sense that it does not alter the equation of state and also has little effect on the fluid viscosity.

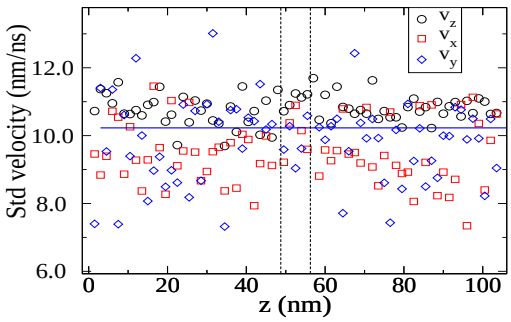

FIG. 2: (Color online) Standard deviation of the three components of the local cell velocity along the coupling direction (z). The fluid is argon at mass density $\rho = 0.6$ gm/mol. The horizontal dashed line is the theoretical value at the imput temperature $T = 300K$, given by $[k_B T/(V_c \rho)]^{1/2}$, where the volume of one cell is $V_c = 37500 \mathring{A}^3$. The MD region is shown between vertical dashed lines.

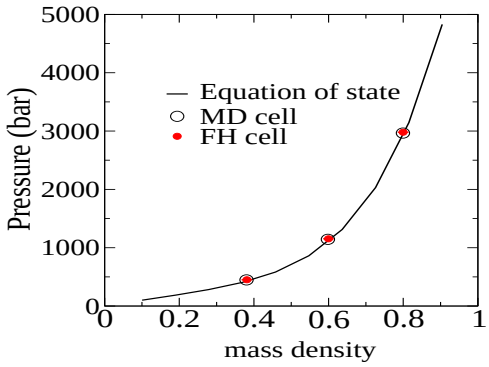

FIG. 3: The mean pressure versus the mean mass density ρ for argon. The equation of state is that of Johnson *et al.* [36] corrected for the contribution of the switched potential added in MD code ($P_{switch} = -250.8\rho^2$ bar). Density is given in gr mol$^{-1}\mathring{A}^{-3}$(= 1.687 gr/cm^3).

2. *Thermodynamic pressure.*

Thermodynamic and hydrodynamic consistency between the molecular and mesoscopic liquid descriptions requires an accurate evaluation of the equation of state. We have measured the pressure relation $p = p(\rho, T)$ for argon and water. Details are given in the Appendix D (see also [17]). Figure 3 shows the pressure at MD and FH for argon at different densities and $T = 300$K; differences are negligible (less than 0.1%).

3. *Density fluctuations.*

Density fluctuations provide a more difficult test for thermodynamic consistency. Each cell can be considered as an open system with (variable) mass M_c and fixed volume V_c exchanging mass and energy with the rest of the system, which acts as a reservoir at fixed temperature T and pressure P. In the thermodynamic limit, the fluctuation of mass at each cell at equilibrium should behave according to the Grand-Canonical (GC) ensemble $\mu V_c T$, where the chemical potential μ is fixed by the reservoir's value $\mu = \mu(T, P)$. According to standard thermodynamics [37], the mass density variance at one cell is given by $\sigma_\rho = \sqrt{(\rho k_B T)/(V_c c_T^2)}$ where $c_T^2 \equiv (\partial P/\partial \rho)_T$ is the sound velocity at constant temperature. Figure 4 compares the theoretical thermodynamic result for the standard deviation of density with numerical results obtained at MD and FH cells, as a function of the mean density.

While at the FH cells the standard deviation of density σ_ρ agrees with the GC value, at the MD cells we observed a deviation which grows with increasing densities. For instance, in the case of argon, we find an excellent agreement between σ_ρ^{MD} and the GC value, for $\rho < 0.5$ but at larger densities σ_ρ^{MD} start to become larger than the GC result (up to about 20% at $\rho = 0.8$ gr/mol/$\mathring{A}^3$). In order to assess whether such discrepancy arises from the mass coupling method or from the intrinsic behaviour of the molecular dynamics, we performed a set of standard MD simulations used as tests. In these test we used rather long periodic boxes (about 17nm) with lateral dimensions (5×5 nm) similar to those used in the hybrid simulations. The large MD box is sliced in smaller cells with sizes similar to those used in the hybrid simulation (1.5 nm). We then measured the variance of mass within each slice. Results, in Fig. 4, show similar deviations from the GC limit, indicating that the deviations observed in the hybrid MD cells are probably intrinsic to the molecular behaviour at such small portions of fluid. The behaviour of mass fluctuations in small dense systems is actually the origin of an interesting debate in the literature [38, 39], which suggest some kind of reformulation of the FH equations for the nanoscale. Here we note that further research on this issue is also relevant for the fine tuning of the hybrid methodology.

4. *Stress fluctuations.*

As stated in Sec. III, in order to evaluate the MD part of the stress tensor in Eq. 12, $\boldsymbol{J}_P^{\boldsymbol{g}}$, one can either introduce the coarse-grained MD variables (density and

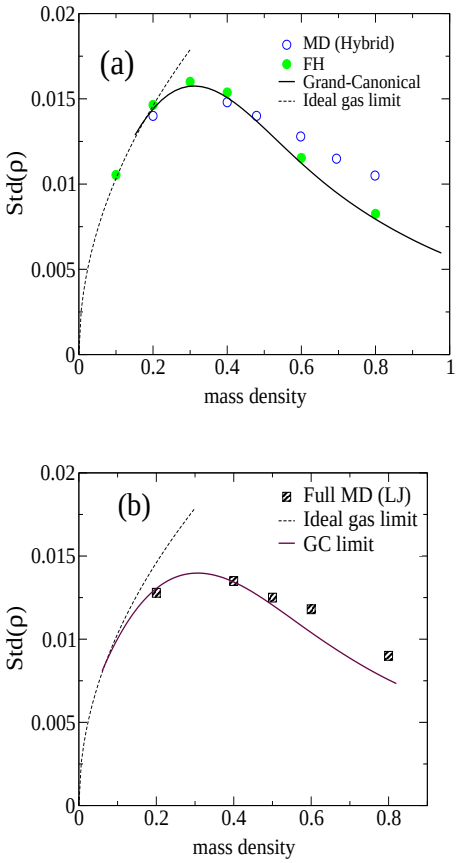

FIG. 4: (a) Standard deviation of the mass density versus the mean mass density for argon. The result for the Grand-Canonical ensemble is $[\rho k_b T/(V_c c_T^2)]^{1/2}$, where $c_T^2 = (\partial P/\partial\rho)_T$ is the squared isothermal sound velocity. Results at FH and MD cells are shown. (b) Results obtained in full MD simulations using large simulation boxes (see text). The argon model used in (b) (simple LJ [36]) has a lower compressibility with respect to (a) arising from a pressure excess of $\delta p(\rho) = 250\rho^2$ bar, see Fig. (3). Density is given in units of gr/mol/$\mathring{A}^3$.

velocity) into the discretized Newtonian constitutive relations [Eqs. (2) and (9)] or, evaluate the MD stress from its microstate, using the kinetic theory formula given in Eq. (15). The first, "mesoscopic", approach is faster and could be useful for many problems where a mesoscopic description of stress fluctuations is valid enough. Using this approach, we checked that, provided that the variance of momentum is similar, stress fluctuations take similar values at the MD and FH regions. This is illustrated in Fig. 5a where we show the standard deviation of the shear stress arising from this kind of coupling.

However, if one needs to capture the real stress fluctuations from the MD side one should use the "microscopic" formulation for the momentum flux tensor $\boldsymbol{J}_P^{\boldsymbol{g}}$ appearing in Eq. (12). This could be necessary in those phenomena driven by stress fluctuations, such as nucleation, interface instabilities, etc... When using the microscopic stress, one needs to be sure that the transport coefficients arising from the Green-Kubo expressions coincide at the molecular and fluctuating hydrodynamics domains. This issue is explained in the Appendix A and we defer a more detailed discussion for a forthcoming work. Figure 5b shows the standard deviation of the shear stress and the normal stress for each cell of a hybrid simulation in which the microscopic stress tensor has been coupled at the interface H. In this case (argon at $\rho = 0.6$ gr/mol/$\mathring{A}^3$ at $T = 300$K) we choose $\Delta t_c = 250 fs$, which is roughly equal to twice the decorrelation time of the stress tensor $2\tau_c$ (see Appendix A).

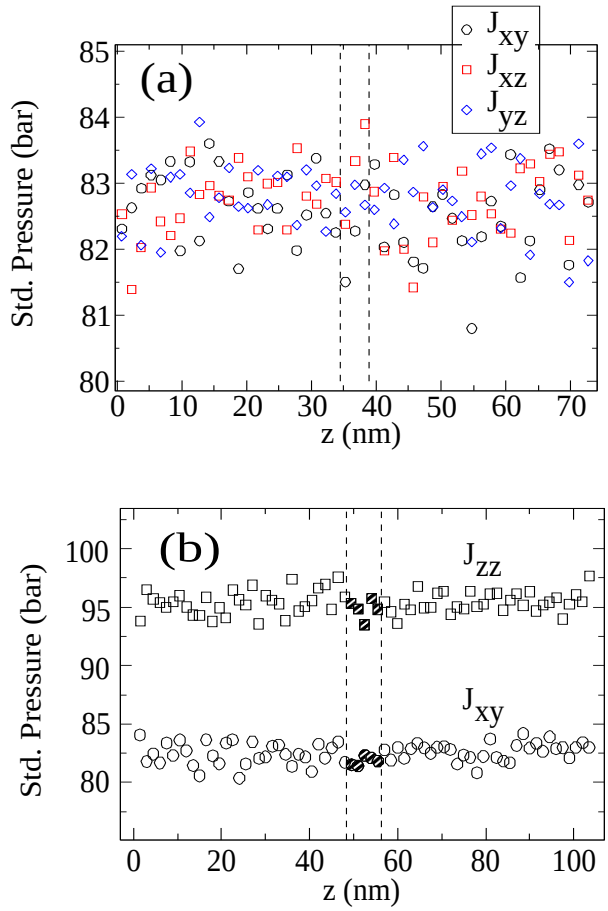

FIG. 5: (Color online) The standard deviation of the pressure tensor components at different cell locations. Results corresponds to argon at $\rho = 0.6$ gr/mol/$\mathring{A}^3$ and $T = 300$K. Cells pertaining to the MD domain are located between dashed the lines. Coupling time is $\Delta t_c = 250$fs and $n_{FH} = 5$ and $n_{MD} = 25$. (a) Results for the off-diagonal components of the pressure tensor using the mesoscopic approach for the pressure tensor within the MD domain (see text). (b) Results for diagonal and off diagonal components of the stress tensor obtained when the microscopic stress tensor is used at the MD domain.

VI. NON-EQUILIBRIUM SIMULATIONS

A. Transversal momentum: start-up of Couette flow.

We performed several tests under non-equilibrium unsteady states which comprise transport of transversal momentum (shear) and longitudinal momentum (sound). Figure 6 illustrates a simulation of the start-up of a Couette flow in argon at $\rho = 0.6\text{gr/mol}/\mathring{A}^3$ and $T = 300$ K. Figure shows the transversal velocity isocontours of a spatio-temporal diagram (space in coordinates and time in abscissas). Comparison is made between the purely fluctuating hydrodynamic solution (called "Hydro" in Fig. 6) and the hybrid MD-FH solver ("Hybrid"). For this comparison, in Fig. 6, we used the same sequence of random numbers for feeding the fluctuating stress in the Hydro and Hybrid FH cells. We also checked that, in terms of second order statistics, both solutions are indistinguishable.

Figure 7 shows the final steady state of the Couette flow. The velocity profile perfectly matches the expected linear profile. As an aside, the reader might be interested in comparing Fig. 7 with Fig. 10, where the viscosity at the FH side is not correctly calibrated with the molecular one. As long as our scheme conserves momentum, in this latter case a zig-zag velocity profile is produced, whose slopes can be used for measuring the proper molecular viscosity (see Appendix D 2).

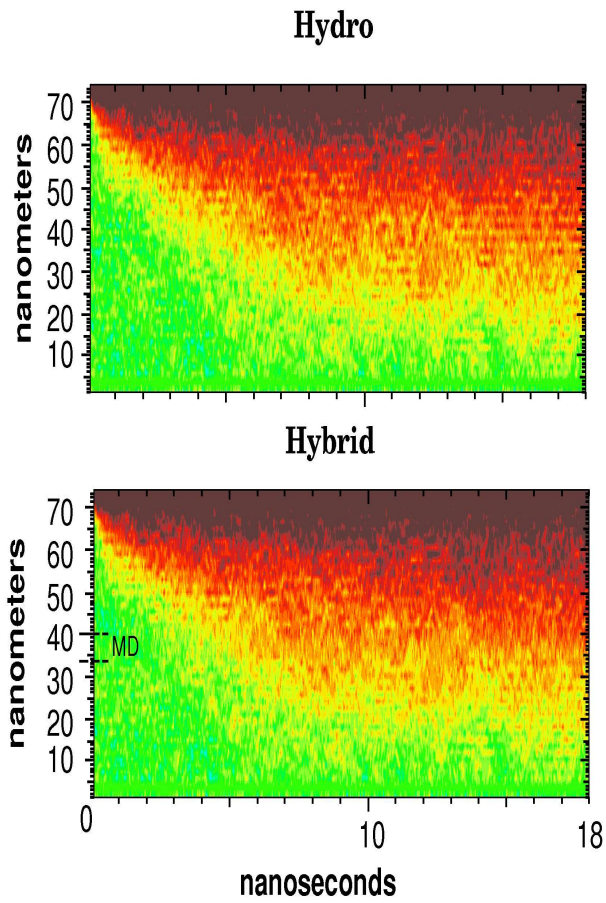

FIG. 6: (Color online) Spatio-temporal diagram showing the start-up of a Couette flow. "Hydro" denotes results from the fluctuating hydrodynamic model (FH) and "Hybrid" from the hybrid MD-FH simulation (the MD region is indicated between the horizontal dashed lines). The velocity imposed at the upper wall is 1 $\mathring{A}$/ps and bottom wall is at rest.

B. Longitudinal momentum: sound waves.

One of the important novelties of the present hybrid scheme is its ability to solve sound waves. In a previous work we presented some stringent tests to the hybrid scheme by considering sound waves of water colliding against a lipid monolayer. Fully fledged MD results were shown to agree with those obtained by the hybrid code. Interestingly, far away from the wall, the reflecting wave still differed from that reflected against a purely reflecting wall (solved by fluctuating hydrodynamics). This fact indicates that the model is able to capture fine differences arising from the molecular structure near an interface. In this work we show another test which intends to illustrate the time-resolution of the model.

We consider a closed box with rigid, reflecting walls and introduce a density perturbation near one of the walls of the box. The box is periodic in x and y direction and walls are located at $z = z_0$ and $z = z_1$. In this simulations the MD region is located at the bulk of the fluid (center region of the box) and it surrounded by the FH model. As a consequence of the initial perturbation two sound waves start to travel in opposite directions. But as the initial density perturbation is maxima near one of the walls, one of the sound waves is soon reflected by the wall, changing its sense of propagation. The result is two density peaks moving at the speed of sound in the same direction. These two peaks can be seen in Fig. 8, where a spatio-temporal diagram of such wave is shown. A quite good agreement is found between hybrid hydrodynamics and purely fluctuating hydrodynamic results. The main conclusion is that the hybrid algorithm is able to correctly resolve flow features separated by quite small time delays. In the simulation of Fig 8, the time delay of both density peaks is 0.02 ns.

Figure 9 shows the time-evolution of the density at the center MD cell, corresponding to the same wave as in Fig. 8. Comparison with deterministic and purely fluctuating hydrodynamics is made. A quite good agreement is observed. We note that fluctuations around the deterministic solution have higher frequency components for the MD cells of the hybrid case (see Fig. 8). This is due to the fact that density fluctuations with wavelengths smaller than few cells cannot be transferred to the FH domain and dissipate within the MD domain. Further study on this high frequency fluctuations is deferred for future work.

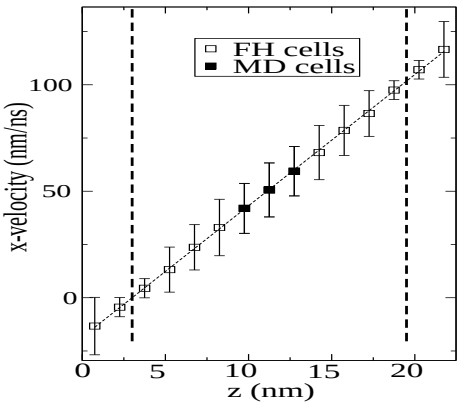

FIG. 7: Steady solution of the Couette flow velocity. Error bars indicate the standard deviation of the velocity within each cell, which corresponds to that of argon at $\rho = 0.6$ gr/mol/$\mathring{A}^3$ and temperature $T = 300$ K. The viscosity, $\eta = 7.50 \times 10^{-5}$ Pa s was previously calibrated using the hybrid setup (see Appendix D 2).

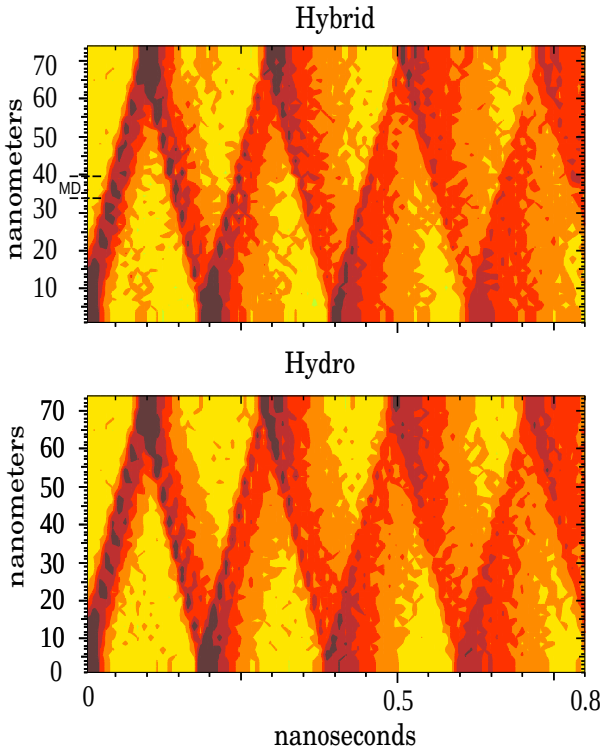

FIG. 8: (Color online) Spatio-temporal diagram showing the evolution of a density wave within a closed box. Comparison is made between results from the fluctuating hydrodynamic model ("Hydro", at bottom) and from the hybrid MD-FH model ("Hybrid", at top). The MD region is located at the center of the box, as indicated. The system is divided in 49 control cells, aligned in z-direction, with dimensions $50 \times 50 \times 15$ $\mathring{A}^2$. The mean density is about ρ =0.6 gr/mol/$\mathring{A}^3$. Upon the initial perturbation the maximum and minimum densities are 0.85 and 0.55 gr/mol/$\mathring{A}^3$, providing an initial Mach number ($\mathrm{Ma}^2 \sim \Delta\rho/\rho$) of about Ma=0.7.

VII. SUMMARY AND CONCLUSIONS

We have presented a detailed account of the multiscale model for hybrid particle-continuum simulations[10]. Our formalism is based on conservation laws (exchange of fluxes of conserved quantities across the interface dividing both subdomains). The present code includes important features so far lacking in the literature, which we now briefly summarize.

The molecular region is described by an all purpose atomistic model which enables to treat the interaction of complex molecules with fluid flow, such as biological macromolecules in aqueous solvent and external hydrodynamic fields [40]. Also, proper consideration of fluctuations is made. Although fluctuations play an important rôle in many different processes, most previous hybrid particle-continuum models do actually try to suppress the effect of fluctuations coming from the MD domain (the problem of noise reduction). Here we consider fluctuations as an important part of the hybrid coupling and we consistently treat the coarse-grained solvent region via fluctuating hydrodynamics (FH). The FH equations (for water and argon) were solved by an Eulerian reference using the finite volume method. For details of this FH code we refer to [17]. Mean values and variances of hydrodynamic variables were shown agree at both sides of the hybrid interface. We found however that at liquid densities ($\rho > 0.5$ gr/mol/$\mathring{A}^3$, in argon) the fluctuation of mass in the MD domain slightly deviates from the thermodynamic limit established by the Grand-Canonical ensemble. Similar deviations were found to occur in standard MD simulations, so these are probably intrinsic to the fluid behaviour at small scales.

Concerning non-equilibrium states, an relevant ability of the scheme is to resolve sound. The scheme provides an exact balance of mass transfer across the interface which permits to transfer high frequency sound waves across the interface. We note that the present version of the hybrid model does not consider energy transport and we worked in isothermal environment. Thus we worked with high frequency isothermal waves, for which the thermal diffusion time is of the same order of the sound period [10]. For a general description of sound one would need to include the energy equation in the hybrid coupling. The work by Flekkøy *et al.* [18] actually provides a one-way energy coupling; a two-way energy coupling will be considered in future work.

Some general remarks on the hybrid methodology are finally made. We believe that the present work is an relevant step towards the completion of the physical formalism for multiscale hybrid schemes based on domain decomposition. However, the hybrid methodology still requires to consider several computational issues to become a standard tool in molecular simulations. In particular, parallelization of the hybrid set-up is needed (both

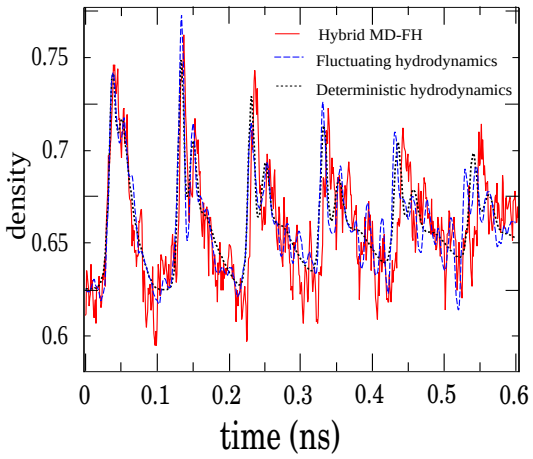

FIG. 9: (Color online) The temporal evolution of the density at the center MD cell in a simulation of a sound wave reflecting within a closed box (argon at $T = 300$K). Comparison is made between the hybrid solution and those obtained using deterministic and fluctuating hydrodynamics with similar initial conditions. Density in units of gr/mol/$\AA^3$.

within the MD domain and also the communications with the continuum domain). The hybrid model will also benefit from new ideas from both computational and simulation fields: faster molecular dynamics codes based on new processor architectures like the Cell processor [41] will reduce the computational burden of the MD from respect the continuum model of at least one order of magnitude; innovative solutions to switch from the atomistic to coarse-graining models [42] may help to transfer complex molecules across the interface; and finally research on "hybridization" of complex 3D geometries will enable more flexibility in the hybrid set-up.

VIII. ACKNOWLEDGMENTS

R.D-B acknowledges funding from the Spainsh projects CTQ2004-05706/BQU, FIS2004-01934 and from additional funding of Ramon y Cajal Research Contract.

APPENDIX A: TIME AVERAGING AND STRESS TENSOR FLUCTUATIONS

We now explain how to perform local time averages of the pressure tensor exchanged between the two models (MD and FH) at the P and C cells ($\boldsymbol{J}^{\boldsymbol{g}}_P$ and $\boldsymbol{J}^{\boldsymbol{g}}_C$ respectively, see Eq. (12)). In doing so one needs to take into account the following constraints: first, the amplitude of stress fluctuations should coincide at the MD and FH sides $\langle[\delta \boldsymbol{J}^{\boldsymbol{g}}_{MD}]^2\rangle = \langle[\delta \boldsymbol{J}^{\boldsymbol{g}}_{FH}]^2\rangle$ and second, the dissipation rates associated to the Green-Kubo relations should agree at both sides.

In the following we consider the equilibrium state ($\langle J\rangle = 0$ and $\delta \boldsymbol{J} = \boldsymbol{J}$) and work with the Green-Kubo relation involving the off diagonal part of the pressure tensor, $J = J^{\boldsymbol{g}}_{xy}$ (similar conclusion is obtained using any other component). In general, the Greek-Kubo relation can be casted in the form,

$$\langle J(0)^2\rangle = \frac{\eta k_B T}{V\tau_c} \tag{A1}$$

where we have defined the decorrelation time,

$$\tau_c \equiv \frac{\int_0^\infty \langle J(t)J(0)\rangle dt}{\langle J(0)^2\rangle} \tag{A2}$$

From the MD side one gets that for simple liquids $\tau_c \sim$ 100fs. At the FH side Eq. (A1) provides [16, 17], $\langle J^2_C\rangle = 2\eta k_B T/(V\Delta t)$. Thus, for the FH model the decorrelation time is $\Delta t/2$.

Now, if the variance of stress fluctuations at MD and FH sides should be equal ($\langle J^2_P\rangle = \langle J^2_C\rangle$) and still both being consistent with the Green-Kubo formula in Eq. (A1); then their decorrelation times should also coincide, i.e., $\Delta t = 2\tau_c$. This means that that the time interval $2\tau_c$ is actually the smallest possible coupling time. In fact, smaller values of Δt would not be consistent with the Markovian assumption, implicit in the FH model.

One can of course use larger coupling times. In general we set $\Delta t_c = n_{FH}\Delta t = N_s \delta t_s$, where the MD sampling time δt_s is made equal to $\delta t_s = 2\tau_c$. At the MD side, the stress tensor is evaluated according to Eq. (15), while at the FH side one needs to average the stress tensor as, $\langle J_C\rangle_{[\Delta t,\Delta t_c]}$, using the time average defined in Eq. (16). From the Green-Kubo expressions it is not difficult to show that the variance of both averages $\langle J_P\rangle_{[\delta t_s,\Delta t_c]}$ and $\langle J_C\rangle_{[\Delta t,\Delta t_c]}$ coincide, being both proportional to $1/\Delta t_c$.

In the present simulations we have used $\Delta t_c = 2\tau_c$, for which $N_s = 1$, so the time average in Eq. (15) reduces to the instantaneous value at $t + \Delta t_c$. At the FH side we used values of n_{FH} ranging from 3 to 5.

APPENDIX B: THE BUFFER DYNAMICS

In this appendix we comment on the choice of the distribution of the external force $\boldsymbol{F}_H$ over the particles at the buffer B. As stated, each particle at the buffer feels a force $\boldsymbol{f}^{ex}_i$ such that $\sum_{i\in B} \boldsymbol{f}^{ex}_i = \boldsymbol{F}_H$. In principle, the force per particle $\boldsymbol{f}^{ex}_i$ may be distributed according to any distribution g_i, such that

$$\boldsymbol{f}^{ex}_i = \frac{g_i \boldsymbol{F}_H}{\sum_{i\in B} g_i} \tag{B1}$$

Several values of g_i have been proposed in the literature. For instance, Flekkøy *et al.* [26] proposed $g_i = g(r^\perp_i)$ where $r^\perp_i = \boldsymbol{r}_i \cdot \boldsymbol{e}_\perp$ is the coordinate normal to H. In order to prevent particles from escaping out from the particle system they chose a function $g(r^\perp)$ diverging at a certain distance from H and tending to zero at H. Werder and Koutmoutsakos [30], showed that an evaluation of

$g(r^\perp)$ from a previous calculation of the particle distribution function in the $r_\perp$ coordinate, enables to maintain a constant density profile across the whole buffer (a comparison between several choices of g_i was also provided). In a previous work [27] we used $g_i = 1$ in order to keep under control the average energy dissipated by the external force. Note that energy dissipation increases like $\boldsymbol{f}_i^{ex}\boldsymbol{v}_i$ so any increasing function $g(r)$ will substantially increase energy production [27]. This dilemma was solved in a subsequent work [18], where an elegant method for momentum and energy flux boundary conditions was derived. This method introduces a fluctuating force which depends on the particle velocities. In other words, $g_i = 1+g_i'(\{\boldsymbol{v}_i\})$ where g_i' provides the fluctuating component of the external force ($\sum_{i\in B} g_i'(\{\boldsymbol{v}_i\}) = 0$) and ensures that the *exact* amount of energy is released into the system (not only in average).

Based on our experience, the most important issue in deciding the shape of the distribution g_i is to ensure a flat density profile $\rho(r^\perp)$ around the interface H, at least over distances of several cutoff radius $> O(\sigma)$. This requirement is particularly important when dealing with longitudinal flow (like sound waves) because density gradients generate longitudinal currents. Using the information from previous works we used,

$$g_i = g(r_i^\perp) = \begin{cases} 0 & \text{if } |r_i^\perp - r_H^\perp| < \delta \\ 1 & \text{if } |r_i^\perp - r_H^\perp| \geq \delta \end{cases} \tag{B2}$$

where $\boldsymbol{r}_H$ is the position of the H interface and δ is a distance of several particle radius $\delta \sim 3\sigma$ (in particular $\delta = 9\mathring{A}$). The total length of the buffer in the $r^\perp$ direction was set to $15\mathring{A}$ (about 4 particle radius).

The resulting density profile $\rho(r^\perp)$ is illustrated in Ref. [10] in the case of (TIP3P) water. Within the buffer, the density profile is flat over distance of about 3σ which proves to be suffiently large to avoid spurious longitudinal currents at the interface H. By constraining $g = 1$ only to the outer part of the buffer while making $g = 0$ near the interface H, we could avoid fluid layering (wavy density profile) around H. Moreover using $g = 1$ the heat produced by the external force was easily thermalized.

APPENDIX C: EXACT MASS AND MOMENTUM CONSERVATION

This section provides a modification of the scheme which enable to achieve an exact momentum conservation. The idea is to adjust the momentum transfer towards each C cell so as to ensure global conservation along the interface contour. The method is general and can be applied to any conserved scalar quantity (in particular to any component of the momentum). Let ϕ be this conserved quantity and $\Delta\phi_{MD}$ its net change within the MD system over the time interval $[t_0, t_1]$ with $t_1 = t_0 + \Delta t_c$. As explained in Sec. IV the MD model is the first to be moved from t_0 to t_1, so $\Delta\phi_{MD} = \phi_{MD}(t_1) - \phi_{MD}(t_0)$ is known before the FH field is updated. Local conservation implies that the amount of ϕ crossing the hybrid interface towards the FH domain is $-\Delta\phi_{MD}$. In a general setup (see Fig. 1b), the interface H is divided in $h = \{1, ..., \mathcal{N}_\mathcal{H}\}$ surface portions. Each portion h is facing a different C_h cell. Thus conservation implies,

$$\sum_{h\in H} \delta\phi_h = -\Delta\phi_{MD} \tag{C1}$$

where $\delta\phi_h$ is the amount of ϕ crossing the portion h of the interface H towards the corresponding C_h cell. The hydrodynamic prediction for $\delta\phi_h$ is

$$\delta\phi_h^{\text{pred}} = -A_h \boldsymbol{J}_h^\phi \cdot \boldsymbol{e}_\perp \Delta t_c \tag{C2}$$

where A_h is the area of the h portion of H and $\boldsymbol{J}_h^\phi$ the local flux (as in Fig. 1 $\boldsymbol{e}_\perp$ points to MD). However, particle fluctuations will induce a slight disagreement between the molecular flux of ϕ and the continuum prescription. The overall disagreement is,

$$E[\phi^{\text{pred}}] = \left[(-\Delta\phi_{MD}) - \sum_{h\in H} \delta\phi_h^{\text{pred}}\right] \tag{C3}$$

In order to fulfill the conservation constraint in Eq. (C1) the amount of ϕ crossing the portion h of the interface can finally be set to,

$$\delta\phi_h = \delta\phi_h^{\text{pred}} + \frac{1}{\mathcal{N}_\mathcal{H}} E[\phi^{\text{pred}}] \tag{C4}$$

Equation (C4) provides the set $\{\delta\phi_h\}$ that should be inyected into the corresponding C_h cells as a (Dirichlet) boundary condition along the time interval $[t_0, t_1]$. In this way an exact conservation of ϕ across the hybrid interface is ensured. The present correction might be useful when dealing with complicated hybrid domains in 2D or 3D, composed by many interfacing cells.

APPENDIX D: THERMODYNAMICS AND TRANSPORT PROPERTIES OF THE FLUID

Thermodynamic and hydrodynamic consistency between the molecular and mesoscopic liquid descriptions requires an accurate evaluation of the equation of state $p = p(\rho, T)$ and the transport coefficients (viscosities) of the fluid, from molecular dynamics. There are several ways to obtain the fluid properties; in particular the equation of state might be obtained from equilibrium MD simuations within a periodic domain, either in the isothermal NVT or isobaric NpT ensembles. Also, the fluid viscosity can be measured in equilibrium simulations via the Green-Kubo relation, or from the relation between the stress and the velocity gradient in non-equilibrium simulations (e.g., from a Couette flow).

In this section we show that the present hybrid protocol can be used as an efficient tool for these calibration purposes.

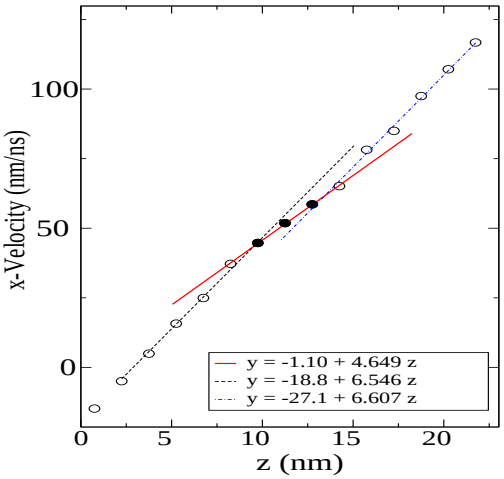

FIG. 10: Calculation of the shear viscosity of argon at $\rho = 0.6$ gr/mol/$\AA^3$ and $T = 300$ K using the hybrid code. The guess value for the viscosity at the FH domain is $\eta_{FH} = 5.31 \times 10^{-5}$Pa s, the slopes (shear rates) at the MD and FH domain (indicated in the figure) provide $\eta_{MD} = (\dot{\gamma}_{FH}/\dot{\gamma}_{MD})\eta_{FH} = 7.50 \times 10^{-5}$Pa s

1. Equation of state

In order to evaluate the equation of state we simplify the hybrid scheme in what we called the "open MD" set-up. This set up consists on reducing the mesoscopic domain to a simple fluid reservoir which imposes a constant pressure p to the molecular domain. As explained in section III, this pressure is imposed at the buffer B and, as long as the MD system is open, it regulates the density at the MD region towards mechanical equilibrium. In fact, *open MD* consists on an open flux boundary condition for the MD domain. The methodology shares the essential features of the method in Ref. [18], where it was shown that the resulting ensemble is Grand Canonical.

We compared the pressure equation of stated obtained from isothermal, isobaric (NpT) and canonical (NVT) ensembles in peridic boxes (using a Berendsen thermostat) with those obtained using the *open MD* simulation (using a DPD thermostat). Argon and the TIP3P model of water were considered, obtaining a perfect agreement with standard MD simulations in closed (periodic) systems [17]. In summary, the *open MD* set up can be used to extract the equation of state of the fluid.

2. Transport coefficients: shear viscosity

The hybrid scheme can also be used as a rheometer. Consider a liquid for which the shear viscosity is unknown. To accurately calibrate the fluid shear viscosity η we impose a Couette flow in an hybrid simulation whereby the MD region is placed at the centre of a domain (see Fig. 10). Once the steady state is reached the balance of momentum flux establishes that, at the hybrid interface, $\dot{\gamma}_{MD}\eta_{MD} = \dot{\gamma}_{FH}\eta_{FH}$. Here the shear rate is $\dot{\gamma} \equiv (\partial v_x/\partial y)$ and subscripts MD and FH denotes local values at the MD and FH domains. Using a guess value at the FH region η_{FH}, this relation enables to accurately determine the shear viscosity at the molecular region η_{MD} from the slopes of the velocity profiles at MD and FH, $\dot{\gamma}_{MD}$ and $\dot{\gamma}_{FH}$. Figure 10 shows an example of this rheology measurement for argon at $\rho = 0.6$ gr/mol/$\AA^3$ and $T = 300$K, which yields $\eta_{MD} = (7.50 \pm 0.05) \times 10^{-5}$ Pa s. This value coincides with that reported in the literature [43].

[1] M. Karttunen, I. Vattulainen, and A. Lukkarinen, eds., *Novel Methods in Soft Matter Simulations*, vol. 640 of *Lecture Notes in Physics* (Springer-Verlag Heidelberg, 2004).

[2] P. Coveney, G. De Fabritiis, M. H. S. Pickles, and A. Porter, Comp. Phys. Commun. **175**, 389 (2006).

[3] R. Delgado-Buscalioni, P. V. Coveney, G. D. Riley, and R. Ford, Phil. Trans. Roy. Soc. London A **363**, 1975 (2005).

[4] G. Csanyi, T. Albaret, M. C. Payne, and A. D. Vita, Phys. Rev. Lett. **93**, 175503 (2004).

[5] A. S. Lipatov, *The Hybrid Multiscale Simulation Technology: An Introduction with Application to Space and Plasma Physics* (Springer-Verlag New York, Inc., Secaucus, NJ, USA, 2001).

[6] A. Garcia, J. Bell, W. Y. Crutchfield, and B. Alder, J. Comp. Phys. **154**, 134 (1999).

[7] P. Koumoutsakos, Ann. Rev. Fluid Mech. **37**, 457 (2005).

[8] O. B. Usta, A. J. C. Ladd, and J. E. Butler, J. Chem. Phys. **122**, 094902 (2005).

[9] G. Giupponi, G. De Fabritiis, and P. Coveney, J. Chem. Phys **126**, 154903 (2007).

[10] G. De Fabritiis, R. Delgado-Buscalioni, and P. Coveney, Phys. Rev. Lett **97**, 134501 (2006).

[11] X. B. Nie, S. Y. Chen, and M. O. Robbins, Phys. Fluids **16**, 3591 (2004).

[12] N. G. Hadjiconstantinou, J. Comput. Phys. **154**, 245 (1999).

[13] F. Alexander, A. Garcia, and D. Tartakovsky, Computing in Science and Engineering **7**, 32 (2005).

[14] N. G. Hadjiconstantinou, A. L. Garcia, M. Z. Bazant, and G. He, J. Comput. Phys. **187**, 274 (2003).

[15] R. Delgado-Buscalioni, E. Flekkøy, and P. V. Coveney, Europhys. Lett. **69**, 959 (2005).

[16] L. D. Landau and E. M. Lifshitz, *Fluid Mechanics* (Pergamon Press, 1959).

[17] G. De Fabritiis, M. Serrano, R. Delgado-Buscalioni, and P. V. Coveney, Phys. Rev. E **75**, 026307 (2007).

[18] E. G. Flekkoy, R. Delgado-Buscalioni, and P. V. Coveney, Phys. Rev. E **72**, 026703 (2005).

[19] J. Keizer, *Statistical thermodynamics of nonequilibrium processes* (Springer-Verlag, New York, 1987).

[20] M. Serrano and P. Español, Phys. Rev. E **64**, 046115 (2001).

[21] E. Flekkøy, P. Coveney, and G. De Fabritiis, Phys. Rev. E **62**, 2140 (2000).

[22] S. V. Patankar, *Numerical Heat Transfer and Fluid Flow* (Hemisphere, New York, 1980).

[23] A. MacKerell, D. Bashford, M. Bellott, R. Dunbrack, J. Evanseck, M. Field, S. Fischer, J. Gao, H. Guo, S. Ha, et al., J. Phys. Chem. B **102**, 3586 (1998).

[24] L. Kalé, R. Skeel, M. Bhandarkar, R. Brunner, A. Gursoy, N. Krawetz, J. Phillips, A. Shinozaki, K. Varadarajan, and K. Schulten, J. Comp. Phys. **151**, 283 (1999).

[25] T. Soddemann, B. Dunweg, and K. Kremer, Phys. Rev. E **68**, 046702 (2003).

[26] E. G. Flekkøy, G. Wagner, and J. Feder, Europhys. Lett. **52**, 271 (2000).

[27] R. Delgado-Buscalioni and P. V. Coveney, Phys. Rev. E **67**, 046704 (2003).

[28] M. Tysanner and A. Garcia, Int. J. Numer. Meth. Fluids **48**, 1337 (2005).

[29] M. Allen and D. Tildesley, *Computer Simulations of Liquids* (Oxford University Press, 1987).

[30] T. Werder, J. H. Walther, and P. Koumoutsakos, J. Comput. Phys. **205**, 373 (2005).

[31] G. De Fabritiis, R. Delgado-Buscalioni, and P. V. Coveney, J. Chem. Phys. **121**, 12139 (2004).

[32] R. Delgado-Buscalioni and P. V. Coveney, J. Chem. Phys. **119**, 978 (2003).

[33] X. B. Nie, S. Y. Chen, W. N. E, and M. O. Robbins, J. Fluid Mech **500**, 55 (2004).

[34] S. T. O'Connel and P. A. Thompson, Phys. Rev. E **52**, R5792 (1995).

[35] C. P. Lowe, EuroPhys. Lett **47**, 145 (1999).

[36] K. Johnson, J. A. Zollweg, and K. E. Gubbins, Mol. Phys. **78**, 591 (1993).

[37] L. D. Landau and E. M. Lifshitz, *Statistical Physics* (Pergamon Press, 1959).

[38] H. Brenner, Physica A **370**, 190 (2006).

[39] H. C. Ottinger, Phys. Rev. Let.. **97**, 090601 (2006).

[40] G. Baldini, F. Cannone, and G. Chirico, Science **309**, 1096 (2005).

[41] G. De Fabritiis, Comp. Phys. Commun. (2007), in press.

[42] M. Praprotnik, L. D. Site, and K. Kremer, J. Chem. Phys **126**, 134902 (2007).

[43] G. Guo and Y. Zhang, Mol. Phys. **99**, 283 (2001).

[44] M. Serrano, G. De Fabritiis, P. Español, and P.V.Coveney, Mathematics and Computers in Simulation **72**, 190 (2006).

[45] J. Bell, A. Garcia, and S. Williams, arXiv:math/0612324 (2007).

[46] This sum is equivalent to $M_P = \sum_i \chi_P(\boldsymbol{r}_i) m_i$, where χ_P is the characteristic function of the cell P i.e. $\chi_P(\mathbf{r}) = 1$ if $\mathbf{r} \in P$ and 0 otherwise.

[47] As shown in Ref. [17], to ensure the correct "numerical" temperature in the FH model one requires $\Delta t \leq 100$ fs if a simple Euler integrator is used. More elaborated integration schemes [44, 45] enable to increase Δt in one order of magnitude.